

Millijoule-scale narrowband terahertz pulses via phase manipulation of pump laser pulses

Spencer W. Jolly,^{1,2,*} Nicholas H. Matlis,³ Frederike Ahr,^{3,4,5} Vincent Leroux,^{1,2} Timo Eichner,¹ Anne-Laure Calendron,^{3,6} Hideki Ishizuki,⁷ Takunori Taira,⁷ Franz X. Kärtner,^{3,4,6} and Andreas R. Maier¹

¹*Center for Free-Electron Laser Science and Department of Physics Universität Hamburg,*

Luruper Chaussee 149, 22761 Hamburg, Germany

²*Institute of Physics of the ASCR, ELI-Beamlines project,*

Na Slovance 2, 18221 Prague, Czech Republic

³*DESY and Center for Free-Electron Laser Science,*

Notkestraße 85, 22607 Hamburg, Germany

⁴*Department of Physics, Universität Hamburg,*

Luruper Chaussee 149, 22761 Hamburg, Germany

⁵*IMPRS, Hamburg, Germany*

⁶*The Hamburg Center for Ultrafast Imaging,*

Luruper Chaussee 149, 22761 Hamburg, Germany

⁷*Institute for Molecular Science, National Institutes of Natural Science,*

38 Nishigonaka, Myodaiji, Okazaki 444-8585, Japan

Abstract

Electromagnetic radiation at terahertz (THz) frequencies is a useful tool in probing and controlling matter and light in new and interesting ways, especially at high peak-fields and pulse energies. Generating THz radiation often employs nonlinear optical processes, for which the overlapping of stretched, broadband near-infrared (NIR) pulse copies within nonlinear crystals is common. Here we show that for narrowband THz generation, the higher-order phase present on the NIR pulses offers control of the properties of the THz, for example creating temporally complex THz with multiplexed NIR pulses. We manipulate the phase of two NIR pump pulses independently to remove higher order effects and generate record mJ-level THz in two crystals simultaneously, with an average total energy of $604 \mu\text{J}$ at 361 GHz with 1 % bandwidth. This high pulse energy combined with such a narrow bandwidth has broad implications for accelerator applications, resonant driven material studies, and nonlinear THz spectroscopy.

INTRODUCTION

Recent years have seen a tremendous surge in development of terahertz (THz) sources of high energy and high peak-field for applications in compact electron acceleration [1–3], control and metrology of electrons [4], characterization of fs-duration FEL pulses [5, 6], control of dynamics in solids [7, 8], and linear and nonlinear spectroscopy [9]. Single-cycle, broadband THz has produced the highest peak-fields [10–12], but for electron acceleration in dispersive structures [13], resonant pumping of materials, or narrowband spectroscopy, multi-cycle, narrowband pulses are required. Especially for electron acceleration to high energies, high THz pulse energies are necessary, for which laser-driven difference frequency generation (DFG) sources are most promising.

Achieving high conversion efficiencies requires high pump fluence and proper phase matching of the nonlinear process. Quasi-phase-matching (QPM) in periodically poled lithium niobate (PPLN) is a good candidate for narrowband THz generation due to the inherent narrow bandwidth of the phase matching and the high nonlinearity in PPLN [14]. Efficiencies up to 0.1% and energies of $\sim 1 \mu\text{J}$ were achieved using optimized fs pump pulses and cryogenic cooling [15]. But to produce the mJ-level THz pulses needed for acceleration applications, pump pulses up to 1 J are required, and fs pulses in this case are limited by optical damage and nonlinear effects, especially in longer crystals. Chirping (stretching) the NIR pump and overlapping delayed pulse copies (Fig. 1) maintains the required difference frequency content while increasing the optical damage threshold [16, 17].

The chirp-and-delay concept was shown in photo-conductive antennas to produce THz at very low pulse energies [18]. More recent results showed up to $10 \mu\text{J}$ via a tilted pulse-front in bulk lithium niobate [19], up to $20 \mu\text{J}$ in organic crystals [20], and energies of up to $40 \mu\text{J}$ using chirp-and-delay in PPLN with a train of pulses [21]. Chirp-and-delay has also produced mid-infrared radiation in organic and inorganic crystals driven by two different OPAs [22, 23]. In this article we demonstrate chirp-and-delay terahertz generation pumped to the joule-level in large aperture PPLN crystals, with both evidence of temporally separated THz pulses and mJ-level THz pulses due to control of the phase components of the phase matched NIR pump pulses. This represents an increase in narrowband THz pulse energies by an order of magnitude, but also an avenue towards control of the envelope and phase—at high energies—beyond previously shown.

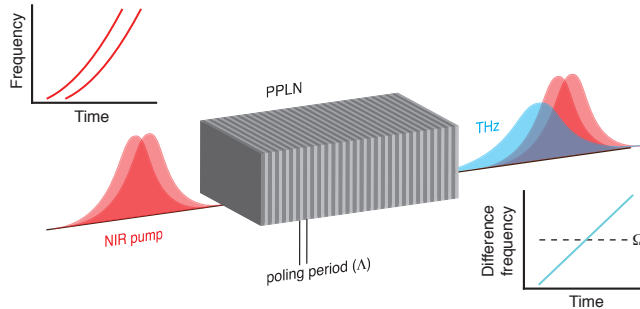


FIG. 1. The concept of chirp and delay in a periodically poled medium. The two chirped pulses with a non-negligible third-order phase are separated in time, and create an angular difference frequency $\Delta\omega$ that is matched to the THz at angular frequency Ω determined by the poling period Λ and material properties of the nonlinear crystal.

RESULTS

Higher-order phase effects

We use stretched pulses from a grating-based Öffner-type stretcher [24], necessary for amplification to the $> 1 J$ pump energies utilized [25]. The second order spectral phase ϕ_2 (or Group Delay Dispersion, GDD) and the third order spectral phase ϕ_3 (third order dispersion, TOD) of the ANGUS laser system (see Methods section) are $\phi_2 = 2.3 \text{ ps}^2$ and $\phi_3 = -0.0044 \text{ ps}^3$ at an 800 nm central wavelength. Calculating the temporal electric field of the delayed and overlapped NIR pump is important for understanding the details of the nonlinear process, in which the TOD plays an important role in determining the phase, temporal structure, and energy of the THz depending on the bandwidth of the process.

Within certain limits the instantaneous angular difference frequency $\Delta\omega$ varies over time, and if the pulses are assumed to be unique, then $\Delta\omega$ is in general quadratic in time

$$\Delta\omega(t) = \alpha + \beta t + \gamma t^2, \quad (1)$$

with each of α , β , and γ depending on the GDD and TOD of each pulse, and temporal delay between them Δt . When the pulses are copies of each other then γ is zero. When the pulses are copies and ϕ_3 is zero, then both β and γ are zero, and $\alpha = \phi_2 \Delta t$ such that $\Delta\omega$ is constant for all time, corresponding to the idealized scenario. However, the magnitude of

TOD from grating-based pulse stretchers causes a significant departure from the ideal [26]. This represents first a drawback, whereby less of the the NIR pump energy is phase matched for the nonlinear process, but also allows the opportunity for control.

Applications of this result include producing THz pulses via difference frequency generation with broadband phase matching that have tunable linear and nonlinear chirp [27], determined by β and γ respectively. Results in this manuscript focus on applications with narrowband phase matching, which include temporally complex THz pulses, and high energy mJ-level THz pulses, both produced via different levels of multiplexing or spectral phase manipulation of the NIR pump pulses.

Temporally complex terahertz

The magnitude of the TOD on chirped-and-delayed pulse copies can create terahertz with a complex and tunable temporal structure. When the difference frequency is only within the phase matching bandwidth in a limited time window, true when β is nonzero, then terahertz can only be produced in a close vicinity to that time determined by the phase matching bandwidth. If the input NIR pump energy is in a longer train of pulses, or if the difference frequency is designed to be phase-matched at more than one time, then the produced terahertz will have complex temporal structure, manifested either as temporal interference or THz pulses completely separated in time.

Experiments use a train of pump pulses produced from a partial-reflective and high-reflective mirror pair [21], with the first two in the train having equal energy, and the following having lower energy (Fig. 2a). These pulses are all copies of each other, excluding the negligible material dispersion of the partial reflector, which results is a significant slope β of the difference frequency. The combination of the slope of the instantaneous difference frequency and the pulse train results in more than one moment in time within the phase matching bandwidth at a given delay (Fig. 2b) corresponding to the matched difference frequency between pulse 1 and pulse 2, and pulse 2 and pulse 3, and so on. We change temporal delay between the pulses in the pulse train to optimize the THz output. Based on calculations a narrow peak is expected without TOD, and when TOD is included the peak is wider, shown in Figure 2c. When both TOD and the pulse train are included the calculation show multiple peaks in the THz output, which is a consequence of the temporally separated

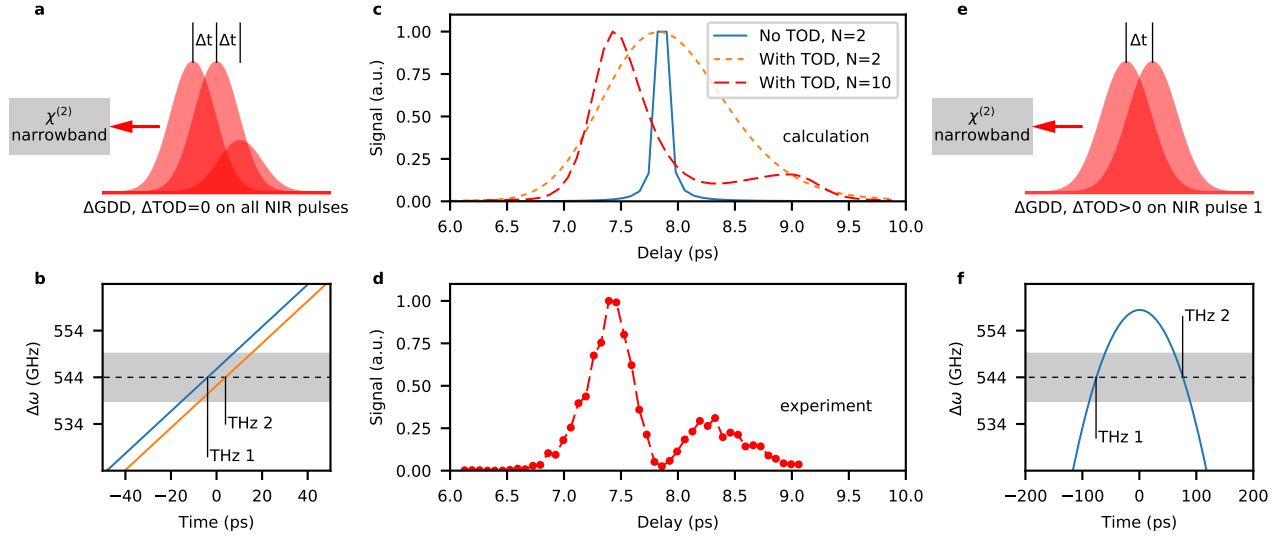


FIG. 2. The production of temporally complex THz pulses. **a**, A train of N identical pulses shown with pulses 1 to 3 and **b**, the instantaneous difference frequency between pulse 1 and pulse 2, and pulse 2 and pulse 3. **c**, Analytic calculations show that the THz output as a function of temporal delay within the pulse train becomes wider when including TOD, and becomes complex when including the pulse-train, which is a result of complex interference between the THz pulses produced at different times shown in **b**. **d**, Experimental observation in a 2 cm long PPLN producing 544 GHz radiation. **e**, A pair of pulses could be engineered with additional GDD and TOD added to only one pulse (15500 fs^2 and 300000 fs^3 respectively) such that isolated THz pulses are generated far apart, as in **f**.

THz pulses interfering in a complex fashion. This agrees with the experimental observation at 544 GHz (Fig. 2d), confirming that temporally separated THz pulses are generated. A similar result was achieved at 860 GHz.

Pushing this concept further, pump pulses could be manipulated separately to have a specific slope and curvature of difference frequency so that THz pulses are generated at a designed temporal separation. An example is shown in Figure 2e–f to have only a quadratic component of difference frequency resulting from positive $\Delta\phi_2$ and $\Delta\phi_3$ on only the first pulse. There is phase matching at two points in time with a separation of about 150 ps.

It is important to note that the longer the crystal the larger an effect group-velocity walk-off will have on the temporally separated THz pulses, causing the THz to extend from the position in time it is initially generated relative to the NIR pump pulses. The pulse

duration of the pump also plays a role, since the temporal extent of the THz from a single phase matching point depends on both the crystal length and pump pulse duration (and indeed the absorption of the crystal) [28]. Closely separated phase matching points (Fig. 2b) produce a single THz pulse with temporal structure, and widely separated phase matching points (Fig. 2f) produce two separate THz pulses, with the intermediate scenarios producing terahertz with two peaks. The experimental results in Figure 2d correspond to the former situation, where the two distinct phase matching regions overlap significantly in time. So-called double-peak THz pulses may have interesting applications to highly controlled particle manipulation, or to specific delayed resonant pumping of materials.

High energy terahertz

We employ the control of pump phase to remove all slope and curvature from the difference frequency in order to be optimally matched to long PPLN crystals having a very narrow acceptance bandwidth. This requires specific manipulation of the GDD and TOD of the pulses separately in order to set β and γ to zero.

The experimental setup for high energy THz generation can be seen in Figure 3. Using a setup similar to a Mach-Zehnder interferometer, we produce two copies of the pulses with a tunable delay when recombined at the exit of the interferometer. The fact that the arms have completely distinct optical paths allows for manipulation of the spectral phase of the pulses independently, which is demanded by the derived solution. Because of the topology of the Mach-Zehnder setup only half of the total input energy can be used to pump a single crystal, but we show that it is possible to pump two crystals simultaneously using both outputs of the setup, since they have identical temporal properties. We use high-dispersion glass prisms to primarily tune the $\Delta\phi_2$, and specially designed high-TOD dispersion compensating mirrors (DCMs) to tune the $\Delta\phi_3$, both detailed in the Methods section.

After the beams are combined they are sent in to the cryostat which has an entrance window AR-coated for the NIR pump beams, and a copper cryo-finger which allows cooling the crystal to below 100 K at a vacuum below 8×10^{-4} mbar. We focus the leak-through of a mirror before the crystal on a CCD and use as a farfield diagnostic to ensure sub- $100 \mu\text{rad}$ pointing offset between the combined beams, crucial for proper phase-matching. The different crystals are detailed in the Methods section, which produce 361 GHz and

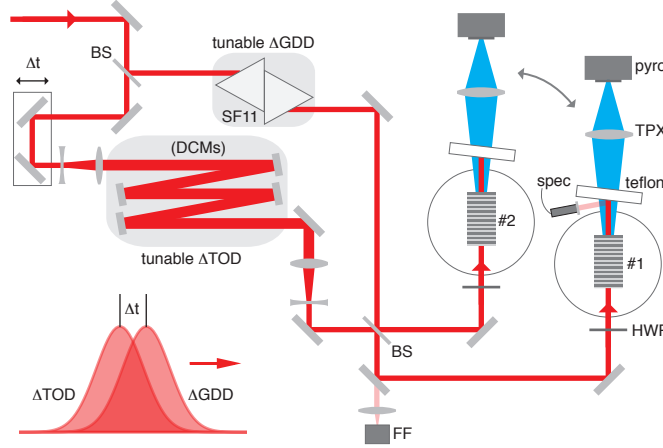


FIG. 3. The experimental setup used to compensate for the effect of third-order phase and to generate THz in two crystals simultaneously. The modification is now to both pulses, and the detection setup is exchangeable between detecting from each crystal. **Key:** BS: beamsplitter; DCMs: dispersion compensating mirrors; FF: farfield camera; HWP: half-wave plate; spec: optical spectrometer; pyro: pyro-electric detector

558 GHz radiation. We mount a ceramic aperture in front of each crystal to avoid clipping of the beam directly on the crystal edges.

The result for 361 GHz is an increase of up to 8 times in the optimal experimental configuration of 47.3 mm SF11 (51.7 mm when telescopes are installed) and 1 TOD mirror compared to the uncompensated case. Two examples of delay scans in Figure 4a show significant narrowing and increase in peak signal. This confirms the picture of the difference frequency flattening over time, since with improved compensation the difference frequency is within the QPM bandwidth for a smaller range of Δt . The output at a constant input fluence for different levels of $\Delta\phi_2$ is shown in Figure 4b. The optimum configuration corresponds to $\Delta\phi_2 = 8800 \text{ fs}^2$ on pulse 1 and $\Delta\phi_3 = 20000 \text{ fs}^3$ on pulse 2. The discrepancy between the measurements and calculations could be due to a number of factors, including the possibility of the high-TOD mirrors having non-zero GDD or contributions of spectral phase terms above third-order. We confirm the narrowband nature of the 361 GHz output to be unchanged from measurements without any phase manipulation.

The result for 558 GHz output from the $212 \mu\text{m}$ poling period crystal is an optimum with $\Delta\phi_2 = 12900 \text{ fs}^2$ on pulse 1 and $\Delta\phi_3 = 60000 \text{ fs}^3$ on pulse 2, with the same plots shown in Figure 4c–d. These results at 558 GHz are consistent, and agree with the prediction of larger

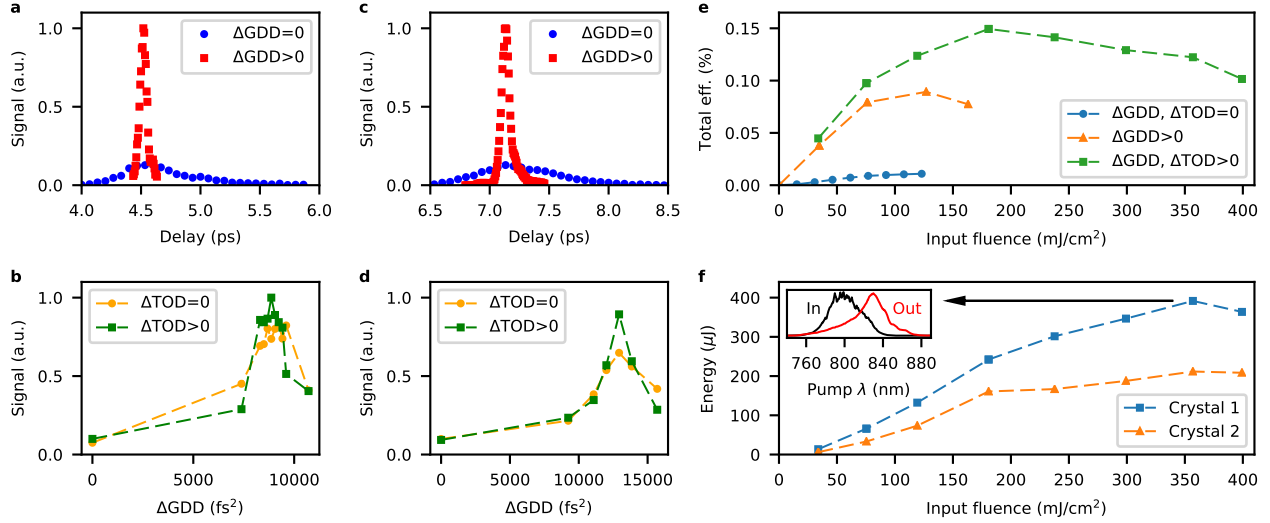


FIG. 4. Optimization of THz output with SF11 material dispersion and high-TOD chirped mirrors. **a**, The comparison of the THz signal with delay for the uncompensated case and the case with 49 mm SF11, and **b**, the maximum THz signal for various amounts of $\Delta\phi_2$ and $\Delta\phi_3$ for the crystal producing 361 GHz radiation. **c–d**, The same shown for the crystal producing 558 GHz radiation. **e**, The THz efficiency in a single 361 GHz crystal as pump fluence is increased in the uncompensated case, with only non-zero $\Delta\phi_2$, and at the global optimum (also with NIR AR coating on both surfaces, and 100 μm glass wafer at the output surface). **f**, The output THz energy from the two crystals simultaneously at 361 GHz, the second of which has no AR coating or wafer installed, with the inset showing the input and output NIR spectrum at the pumping level for highest energy.

$\Delta\phi_2$ and $\Delta\phi_3$ with increasing frequency. Note that at negative delays the output decreases when adding SF11, confirming the unique solution for the optimum Δt .

We pump the two crystals producing 361 GHz radiation simultaneously up to 0.4 J/cm^2 (corresponding to 519 mJ on each crystal before the aperture) and produce a maximum pulse energy of $458 \mu\text{J}$ from the AR-coated crystal with the installed fused silica wafer. The increase in output with each additional level of compensation is shown in Figure 4e. The average energy from this crystal is $392 \mu\text{J}$, and we simultaneously use the second output of the setup to pump the second (uncoated) crystal producing $212 \mu\text{J}$ (Fig. 4f), which is a total average pulse energy of $604 \mu\text{J}$ of THz produced in tandem. This is an additional order of magnitude above previous results with chirp-and-delay, and above any known direct-beam THz produced, especially of such narrow bandwidth. The efficiency begins to saturate above

100 mJ/cm² pump fluence, a behavior similar to previous results pumped at these fluence levels in PPLN [15, 21]. Additionally, above 357 mJ/cm² pump fluence the output THz energy decreases corresponding to a rapid decrease in efficiency. The extreme red-shifting of NIR pump spectrum is shown in the inset of Figure 4f, where the input is centered at 801 nm and the output is centered at 822 nm. Additional results include producing up to an average of 128 μ J pulses at 558 GHz central frequency in the 212 μ m poling period PPLN when pumped to 186 mJ/cm².

DISCUSSION

We have shown that with asymmetric tuning of the second- and third-order phase on overlapped NIR pump pulse copies, control over temporal envelope of generated THz radiation is possible with narrowband phase matching. We showed evidence of temporally complex THz pulses via interference effects when changing the temporal delay between a longer train of pulses, and extrapolated this observation to more extreme cases. We additionally showed that this technique can remove all curvature from the difference frequency in order to fit within the phase matching bandwidth for all time. This produced mJ-level THz pulses, surpassing past results [19–21], and in this case at an even narrower 1% bandwidth. Indeed this technique is general, and especially relevant for the broadband, high energy pump lasers necessary for driving the nonlinear interactions to this extent, which ubiquitously use stretching methods with inherently nonzero higher-order phase [29]. The success of the compensation for the TOD also opens up the tuning or elimination of chirp in high energy THz pulses when produced via broadband phase matching, for example in thin nonlinear crystals.

The optimization and tuning of the energy, chirp, and structure of such narrowband THz pulses has broad implications for accelerator applications, resonant-driven material studies, and nonlinear THz spectroscopy. Although the method shown here does not enable arbitrary control over the narrowband THz waveform, the access to control—especially at such high efficiencies and energies—is unmatched. We believe that the techniques and analyses presented here will become essential tools to push the limits of energy and control in narrowband terahertz and enable applications not yet undertaken.

METHODS

Laser system

For the experiments we used uncompressed pulses from an intermediate amplifier of the ANGUS laser system, a dual-CPA Ti:Sapphire-based laser system operating at 5 Hz and capable of compressed energy up to 5 J and a pulse duration as low as 25 fs. The phase parameters are the same as those used for the analytical underpinnings, $\phi_2 = 2.3 \text{ ps}^2$ and $\phi_3 = -0.0044 \text{ ps}^3$. The beam diameter used is 13 mm with a super-Gaussian profile, and the spectral width is well above 30 nm FWHM centered around 800 nm. The intermediate amplifier used in his work produces pulses with up to 1.2 J energy that have approximately 260 ps duration due to the large bandwidth and GDD.

Experimental phase compensation

SF11 has a group velocity dispersion of $+187.5 \text{ fs}^2/\text{mm}$, so the optimum is expected near 53.3 mm of propagation distance through the SF11 for 361 GHz. Due to the higher quality of DCMs with a high positive TOD as opposed to the negative TOD necessary, we chose mirrors with $+20000 \text{ fs}^3$ per bounce and include them in the opposite arm as the SF11. This results in a different precise solution as initially posed, but in essence it is the same. The TOD per bounce of the high-TOD mirrors was confirmed independently via white-light interferometry measurements. The non-zero TOD of $+126 \text{ fs}^3/\text{mm}$ of the SF11 complicates the situation slightly, but due to the lengths of SF11 used the total amount of TOD from the SF11 is still a small fraction of the total compensation necessary. Therefore, via using variable lengths of SF11 and varying numbers of chirped mirrors we can independently tune the $\Delta\phi_2$ and $\Delta\phi_3$ respectively. In the highest fluence measurements we also installed two identical telescopes to double the size of the beam on the TOD mirrors avoiding optical damage. These telescopes added GDD, which was compensated for by increasing the SF11 in order to stay at the optimum net $\Delta\phi_2$.

The experimental procedure involved changing the distance of SF11 glass by altering the position of the second SF11 prism relative to the first. At each position of the SF11 prisms the position of the beam and path length in that arm changed, which required aligning the beam once more and finding the new optimum temporal delay. At many positions we also

added up to four high-TOD mirrors to find the global optimum.

PPLN crystals

We use $10 \times 15 \text{ mm}^2$ large aperture PPLN crystals [30] with a length of 36 mm. The poling periods of the crystals used are $330 \mu\text{m}$ and $212 \mu\text{m}$, producing 361 GHz and 558 GHz radiation respectively. In addition, on one $330 \mu\text{m}$ poling period crystal the input and output facets were AR coated for the 800 nm pump wavelength, and a $100 \mu\text{m}$ fused silica wafer was attached to the rear surface to attempt to mitigate Fresnel losses for the THz at the rear surface. The other crystals are left uncoated, since we observed severe wavefront distortions from the AR coating on the first crystal when cooled. The performance of the fused silica wafer was also below expectations, likely due to distortions in the wafer when cooled.

ACKNOWLEDGEMENTS

We thank M. Schnepf for help with the laser system, M. Schust and T. Tilp for technical support on the experimental setup, P. Messner for assistance with the vacuum system, K. Ravi for useful theoretical discussions, and S.-H. Chia for help with the white-light interferometry measurements.

We acknowledge support from the European Research Council (ERC) under the European Union Seventh Framework Programme (FP7/2007-2013)/ERC Grant (609920), BMBF grant 05K16GU2, and PIER project PIF-2017-67. S.W. Jolly and V. Leroux were supported by the European Regional Development Fund (ERDF), project ELI-Extreme Light Infrastructure-phase 2 (CZ.02.1.01/0.0/0.0/15.008/0000162).

* spencer.jolly@desy.de

- [1] E.A. Nanni, W.R. Huang, K.-H. Hong, K. Ravi, A. Fallahi, G. Moriena, R.J.D. Miller, and F.X. Kärtner, “Terahertz-driven linear electron acceleration,” *Nature communications* **6** (2015).
- [2] W.R. Huang, A. Fallahi, X. Wu, H. Cankaya, A.-L. Calendron, K. Ravi, D. Zhang, E.A.

- Nanni, K.-H. Hong, and F.X. Kärtner, “Terahertz-driven, all-optical electron gun,” *Optica* **3**, 1209–1212 (2016).
- [3] D.A. Walsh, D.S. Lake, E.W. Snedden, M.J. Cliffe, D.M. Graham, and S.P. Jamison, “Demonstration of sub-luminal propagation of single-cycle terahertz pulses for particle acceleration,” *Nature Communications* **8** (2017).
- [4] C. Kealhofer, W. Schneider, D. Ehberger, A. Ryabov, F. Krausz, and P. Baum, “All-optical control and metrology of electron pulses,” *Science* **352**, 429–433 (2016).
- [5] U. Fröhling, M. Wieland, M. Gensch, T. Gebert, B. Schütte, M. Krikunova, R. Kalms, F. Budzyn, O. Grimm, J. Rossbach, E. Plönjes, and M. Drescher, “Single-shot terahertz-field-driven X-ray streak camera,” *Nature Photonics* **3**, 523–528 (2009).
- [6] I. Grguraš, A.R. Maier, C. Behrens, T. Mazza, T.J. Kelly, P. Radcliffe, S. Düsterer, A.K. Kazansky, N.M. Kabachnik, T. Tschentscher, J.T. Costello, M. Meyer, M.C. Hoffmann, H. Schlarb, and A.L. Cavalieri, “Ultrafast X-ray pulse characterization at free-electron lasers,” *Nature Photonics* **6**, 852–857 (2012).
- [7] M. Först, C. Manzoni, S. Kaiser, Y. Tomioka, Y. Tokura, R. Merlin, and A. Cavalleri, “Nonlinear phononics as an ultrafast route to lattice control,” *Nature Physics* **7**, 854–856 (2011).
- [8] T. Kampfrath, K. Tanaka, and K.A. Nelson, “Resonant and nonresonant control over matter and light by intense terahertz transients,” *Nature Photonics* **7**, 680–690 (2013).
- [9] J. Hebling, K.L. Yeh, M.C. Hoffmann, and K.A. Nelson, “High-power THz generation, THz nonlinear optics, and THz nonlinear spectroscopy,” *IEEE Journal of Selected Topics in Quantum Electronics* **14**, 345–353 (2008).
- [10] M.C. Hoffmann, S. Schulz, S. Wesch, S. Wunderlich, A. Cavalleri, and B. Schmidt, “Coherent single-cycle pulses with MV/cm field strengths from a relativistic transition radiation light source,” *Optics Letters* **36**, 4473–4475 (2011).
- [11] J.A. Fülöp, Z. Ollmann, Cs. Lombosi, C. Skrobel, S. Klingebiel, L. Pálfalvi, F. Krausz, S. Karsch, and J. Hebling, “Efficient generation of THz pulses with 0.4 mJ energy,” *Optics Express* **22**, 20155–20163 (2014).
- [12] C. Vicario, B. Monoszalai, and C.P. Hauri, “GV/m single-cycle terahertz fields from a laser-driven large-size partitioned organic crystal,” *Physical Review Letters* **112**, 213901 (2014).
- [13] L.J. Wong, A. Fallahi, and F.X. Kärtner, “Compact electron acceleration and bunch com-

- pression in THz waveguides,” *Optics Express* **21**, 9792–9806 (2013).
- [14] Y.-S. Lee, T. Meade, V. Perlin, H. Winful, T.B. Norris, and A. Galvanauskas, “Generation of narrow-band terahertz radiation via optical rectification of femtosecond pulses in periodically poled lithium niobate,” *Applied Physics Letters* **76**, 2505–2507 (2000).
- [15] S. Carbajo, J. Schulte, X. Wu, K. Ravi, D.N. Schimpf, and F.X. Kärtner, “Efficient narrow-band terahertz generation in cryogenically cooled periodically poled lithium niobate,” *Optics Letters* **40**, 5762–5765 (2015).
- [16] K.L. Vodopyanov, “Optical generation of narrow-band terahertz packets in periodically-inverted electro-optic crystals: conversion efficiency and optimal laser pulse format,” *Optics Express* **14**, 2263–2276 (2006).
- [17] K. Ravi, D.N. Schimpf, and F.X. Kärtner, “Pulse sequences for efficient multi-cycle terahertz generation in periodically poled lithium niobate,” *Optics Express* **24**, 5253–5276 (2016).
- [18] A.S. Weling, B.B. Hu, N.M. Froberg, and D.H. Auston, “Generation of tunable narrowband THz radiation from large aperture photoconducting antennas,” *Applied Physics Letters* **64**, 137–139 (1994).
- [19] Z. Chen, X. Zhou, C.A. Werley, and K.A. Nelson, “Generation of high power tunable multi-cycle terahertz pulses,” *Applied Physics Letters* **99**, 071102 (2011).
- [20] C. Vicario, A.V. Ovchinnikov, O.V. Chefonov, and C.P. Hauri, “Multioctave spectrally tunable strong-field terahertz laser,” *arXiv 1608.05319* (2016).
- [21] F. Ahr, S.W. Jolly, N.H. Matlis, S. Carbajo, T. Kroh, K. Ravi, D.N. Schimpf, J. Schulte, H. Ishizuki, T. Taira, and F.X. Kärtner, “Narrowband terahertz generation with chirped-and-delayed laser pulses in periodically poled lithium niobate,” *Optics Letters* **42**, 2118–2121 (2017).
- [22] B. Liu, H. Bromberger, A. Cartella, T. Gebert, M. Först, and A. Cavalleri, “Generation of narrowband, high-intensity, carrier-envelope phase-stable pulses tunable between 4 and 18 THz,” *Optics Letters* **42**, 129–131 (2017).
- [23] A. Cartella, T.F. Nova, A. Oriana, G. Cerullo, M. Först, C. Manzoni, and A. Cavalleri, “Narrowband carrier-envelope phase stable mid-infrared pulses at wavelengths beyond 10 μm by chirped-pulse difference frequency generation,” *Optics Letters* **42**, 663–666 (2017).
- [24] G. Cheriaux, P. Rousseau, F. Salin, J.P. Chambaret, B. Walker, and L.F. Dimauro, “Aberration-free stretcher design for ultrashort-pulse amplification,” *Optics Letters* **21**, 414–

416 (1996).

- [25] D. Strickland and G. Mourou, “Compression of amplified chirped optical pulses,” *Optics Communications* **56**, 219–221 (1985).
- [26] S. Kamada, S. Murata, and T. Aoki, “On the chirp of narrowband terahertz pulses generated by photomixing with nonlinearly chirped laser pulse pairs,” *Applied Physics Express* **6**, 032701 (2013).
- [27] S. Kamada, T. Yoshida, and T. Aoki, “The chirp-control of frequency-tunable narrowband terahertz pulses by nonlinearly chirped laser pulse beating,” *Applied Physics Letters* **104**, 101102 (2014).
- [28] Y.-S. Lee, T. Meade, T.B. Norris, and A. Galvanauskas, “Tunable narrow-band terahertz generation from periodically poled lithium niobate,” *Applied Physics Letters* **78**, 3583–3585 (2001).
- [29] S. Backus, C.G. Durfee, M.M. Murnane, and H.C. Kapteyn, “High power ultrafast lasers,” *Review of Scientific Instruments* **69**, 1207–1223 (1998).
- [30] H. Ishizuki and T. Taira, “Half-joule output optical-parametric oscillation using 10-mm-thick periodically poled Mg-doped congruent LiNbO₃,” *Optics Express* **20**, 20002–20010 (2012).